Mid-Wave Infrared High-Speed InAs/GaSb Superlattice Uni-Traveling Carrier Photodetector

Zhijian Shen
School of Information Science and Technology
ShanghaiTech University
Shanghai, China
shenzhj1@shanghaitech.edu.cn

Jinshan Yao
College of Engineering and Applied Sciences
Nanjing University
Nanjing, Jiangsu Province, China
yaojinshan@smail.nju.edu.cn

Hong Lu
College of Engineering and Applied Sciences
Nanjing University
Nanjing, Jiangsu Province, China
hlu@nju.edu.cn

Baile Chen*
School of Information Science and Technology
ShanghaiTech University
Shanghai, China
chenbl@shanghaitech.edu.cn

***Abstract*—We present a UTC-structured high-speed InAs/GaSb T2SL MWIR PD. At 300K, The device has a 4.2 μm zero-bias responsivity of 0.24 A/W and a 4.54 GHz 3-dB bandwidth at -5V.**

Keywords—Mid-wave infrared photodetector, high-speed photodetector, InAs/GaSb type-II superlattice, uni-traveling carrier photodiode

I. Introduction

In recent years, the rapid development and commercialization of fast MWIR sources such as interband cascade lasers (ICLs) [1] and quantum cascade lasers (QCLs) [2] has increased the demand for high-speed MWIR photodetectors (PDs) in a variety of fields, such as free-space communication [3, 4] and frequency comb spectroscopy [5]. Traditional MWIR mercury cadmium telluride (HgCdTe) PDs can only achieve a 3-dB bandwidth of a few hundred MHz [6]. This article presents a high-speed InAs/GaSb type-II superlattice (T2SL) MWIR PD based on a uni-traveling carrier (UTC) structure. At room temperature, the device exhibits a 3-dB bandwidth of 4.54 GHz at -5V when illuminated by a 1550 nm laser source, and its responsivity peaks at 4.2 μm with a value of 0.24 A/W under zero bias; the corresponding peak detectivity is 1.41×10^{8} Jones.

II. Material Growth and Fabrication

The proposed epitaxial structure of the sample wafer is depicted in Fig. 1. By means of molecular beam epitaxy (MBE), the PD structure was grown on an n-type InAs substrate. The epitaxial growth from bottom to top began with a 50 nm n-doped InAs buffer. As an n-contact layer, a 1 μm n-doped InAs layer and 20 periods of n-doped 9.3 nm InAs/1.05 nm AlSb T2SL were then produced. After that, a 400 nm unintentionally doped (uid) InAs drift layer was developed, followed by a 48.66 nm thick uid InAs/AlSb multi quantum well (MQW) relaxation layer to smooth conduction band discontinuities. To achieve better responsivity, the overall thickness of the four-step gradually p-doped 2.4 nm InAs/2.1 nm GaSb T2SL absorption layer increased to 891 nm, as opposed to the thickness of 225 nm in our previously reported InAs/GaSb T2SL MWIR UTC PD [7]. Following that, a 132 nm thick p-doped 1.8 nm AlSb/4.8 nm GaSb T2SL electron barrier layer was grown. Finally, to finish off the whole structure, a 20 nm p-doped InAs p-contact layer was applied.

After material growth, the sample was subsequently manufactured into devices with a circular mesa shape. In order to simultaneously obtain the best sidewall topography and dark current performance, the mesa was created using a hybrid etch process that combined an inductively coupled plasma (ICP) dry etch procedure along with a short-time citric acid-based solution wet etch aftertreatment. Through e-beam evaporation, Ti, Pt, and Au metals were deposited on the p- and n-contact layers to create ohmic contact. The scanning electron microscope (SEM) image of a 20 μm diameter device after metal deposition is shown in Fig. 2. After that, the mesa surface was passivated using SU-8 photoresist. The PDs were lastly connected to gold-plated coplanar waveguide (CPW) pads with 50 Ω characteristic impedance via air bridges for high-speed testing [8].

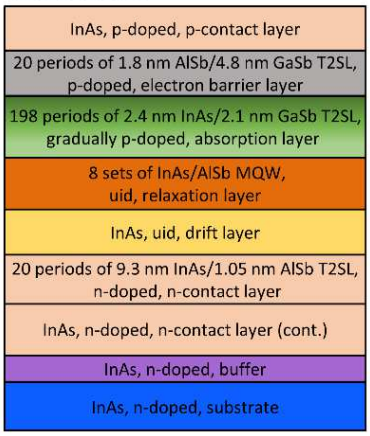

Fig. 1. Illustration of the high-speed InAs/GaSb T2SL MWIR PD sample structure.

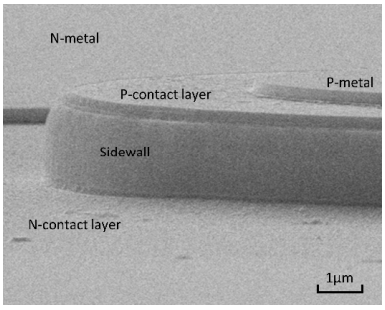

Fig. 2. SEM image of a 20 μm device after p- and n-metal definition.

III. Results and Discussion

Fig. 3 depicts the observed dark current density (J-V) of a device with a diameter of 100 µm as a function of bias voltage at 300 K. The J-V data was taken and examined by a semiconductor device analyzer. At -0.1V, the dark current density is 8.63 A/cm^2.

The sample's responsivity spectra were measured using a Fourier transform infrared (FTIR) spectrometer, and a blackbody source was utilized for calibration. Fig. 4 depicts the responsivity of a 100 µm device subjected to various biases at 300 K. At 300 K, the cutoff wavelength is around 5.6 µm. The responsivity improves as bias increases from 0 V to -1 V and -4 V, albeit at the expense of a worsening signal-to-noise ratio (SNR). The peak responsivity at 4.2 µm under 0 V is around 0.24 A/W. The Johnson-noise and shot-noise limited detectivity of the device D^* is computed as follows [7]:

$$D^* = R_i\sqrt{A}\left(\frac{4k_BT}{R} + 2qI\right)^{-1/2} \quad (1)$$

where R_i is the responsivity, A is the device area, k_B is the Boltzmann constant, T is the temperature of the device, R is the dynamic resistance under corresponding bias, q is the electronic charge, and I is the dark current. Fig. 5 shows the calculated D^* of the device under different biases at 300 K. Under 0V, a peak D^* of 1.41×10^8 Jones was attained. Due to the higher boost in noise than responsivity, the peak D^* drops as bias increases.

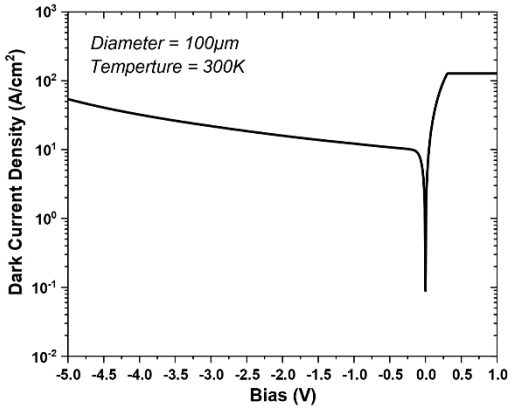

Fig. 3. The relationship between the dark current density and bias voltage for a 100 µm device at 300K.

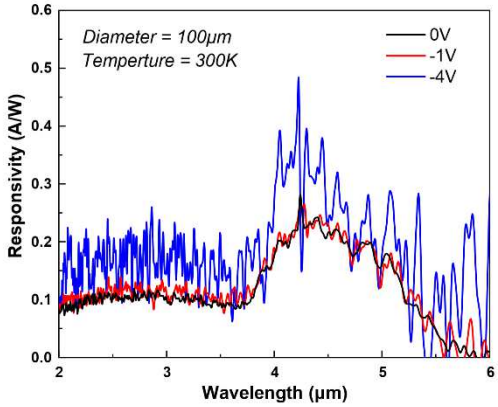

Fig. 4. Responsivity of a 100 µm device under different biases at 300 K.

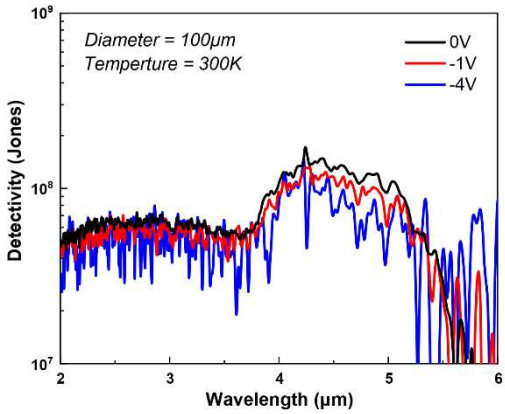

Fig. 5. Johnson-noise and shot-noise-limited detectivity of a 100 µm device under various biases at 300 K.

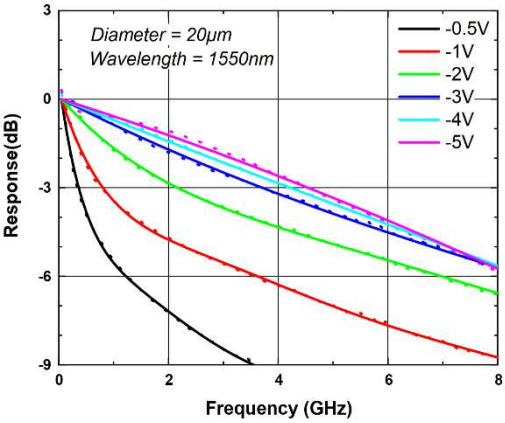

Fig. 6. Frequency response of a 20 µm device under different biases at 300 K when irradiated by a 1550 nm IR laser source.

A lightwave component analyzer (LCA) was used to measure the frequency response of the device at 300K. Focused by a lensed fiber, an intensity-modulated infrared (IR) light at 1550 nm was illuminated on the test devices. A ground-source-ground (GSG) probe was used to collect the photoresponse. The radio frequency (RF) and DC components of the photoresponse were then split by an RF bias tee; the RF signal was returned to the LCA, and the DC component was linked to a source meter, which provides DC bias and monitors photocurrent. It is noteworthy that according to the prior research [7], characterizing using a 1550 nm IR light source instead of a MWIR light source may result in a variation in terms of 3-dB bandwidth, but this difference is usually minimal and can be ignored. The frequency response of a 20 µm device under various biases at room temperature is shown in Fig. 6. Since the drift layer will progressively be entirely depleted when the bias increases from -0.5 V to -3 V, the 3-dB bandwidth rises quickly from 364 MHz to 3.71 GHz. After that, when the bias increases from -3V to -5V, the 3-dB bandwidth improves slightly from 3.71 GHz to 4.54 GHz because the speed of photoexcited electrons in the drift layer will be marginally accelerated. The 3-dB bandwidth might be further increased by using a greater reverse bias; but, as previously noted, this would result in a drop in DC performance in terms of detectivity and dark current. An

extremely high bias voltage will also significantly increase the chance of device breakdown. Table I compares the PD described in this work to the previously reported high-speed MWIR InAs/GaSb UTC device [7].

TABLE I. PERFORMANCE COMPARISON OF UTC-STRUCTURED HIGH-SPEED INAS/GASB T2SL MWIR PDS AT 300 K

Reference	*Responsivity (A/W)*	*Dark current (A/cm2)*	*3-dB bandwidth (GHz)*
This work	0.24	8.63	4.54
[7]	0.1	0.46	6.58
Condition	@ 4.2 μm, 0V	@-0.1 V	@1550 nm, -5V

IV. CONCLUSION

In conclusion, we have successfully demonstrated a high-speed InAs/GaSb T2SL MWIR PD modified from the first prototype device. The device's cut-off wavelength is around 5.6 μm at room temperature, and its responsivity at 4.2 μm and 0 V is around 0.24 A/W. At -5V, the 3-dB bandwidth of a 20 μm detector is about 4.54 GHz.

ACKNOWLEDGMENT

This work was supported in part by the National Natural Science Foundation of China under Grant 61975121, and in part by the Double First-Class Initiative Fund of ShanghaiTech University. We are grateful for the device fabrication support from the ShanghaiTech University Quantum Device Lab.

REFERENCES

[1] I. Vurgaftman *et al.*, "Mid-IR Type-II Interband Cascade Lasers," *IEEE Journal of Selected Topics in Quantum Electronics,* vol. 17, no. 5, pp. 1435-1444, 2011, doi: 10.1109/jstqe.2011.2114331.

[2] Y. Yao, A. J. Hoffman, and C. F. Gmachl, "Mid-infrared quantum cascade lasers," *Nature Photonics,* vol. 6, no. 7, pp. 432-439, 2012, doi: 10.1038/nphoton.2012.143.

[3] C. Liu *et al.*, "Free-space communication based on quantum cascade laser," *Journal of Semiconductors,* vol. 36, no. 9, 2015, doi: 10.1088/1674-4926/36/9/094009.

[4] A. Soibel *et al.*, "Midinfrared Interband Cascade Laser for Free Space Optical Communication," *IEEE Photonics Technology Letters,* vol. 22, no. 2, pp. 121-123, 2010, doi: 10.1109/lpt.2009.2036449.

[5] L. A. Sterczewski *et al.*, "Mid-infrared dual-comb spectroscopy with interband cascade lasers," *Opt Lett,* vol. 44, no. 8, pp. 2113-2116, Apr 15 2019, doi: 10.1364/OL.44.002113.

[6] G. Perrais *et al.*, "Study of the Transit-Time Limitations of the Impulse Response in Mid-Wave Infrared HgCdTe Avalanche Photodiodes," *Journal of Electronic Materials,* vol. 38, no. 8, pp. 1790-1799, 2009, doi: 10.1007/s11664-009-0802-7.

[7] J. Huang, Z. Xie, Y. Chen, J. E. Bowers, and B. Chen, "High Speed Mid-Wave Infrared Uni-Traveling Carrier Photodetector," *IEEE Journal of Quantum Electronics,* vol. 56, no. 4, pp. 1-7, 2020, doi: 10.1109/jqe.2020.3003038.

[8] Z. Xie *et al.*, "High-speed mid-wave infrared interband cascade photodetector at room temperature," *Opt Express,* vol. 28, no. 24, pp. 36915-36923, Nov 23 2020, doi: 10.1364/OE.409868.